BIOCHEMISTRY
including biophysical chemistry & molecular biology

Article

pubs.acs.org/biochemistry

Iron Content of *Saccharomyces cerevisiae* Cells Grown under Iron-Deficient and Iron-Overload Conditions

Gregory P. Holmes-Hampton,[†] Nema D. Jhurry,[‡] Sean P. McCormick,[†] and Paul A. Lindahl*[,†,‡]

[†]Department of Chemistry, Texas A&M University, College Station, Texas 77843-3255, United States

[‡]Department of Biochemistry and Biophysics, Texas A&M University, College Station, Texas 77843-2128, United States

Supporting Information

ABSTRACT: Fermenting cells were grown under Fe-deficient and Fe-overload conditions, and their Fe contents were examined using biophysical spectroscopies. The high-affinity Fe import pathway was active only in Fe-deficient cells. Such cells contained ~150 μM Fe, distributed primarily into nonheme high-spin (NHHS) Fe^{II} species and mitochondrial Fe. Most NHHS Fe^{II} was not located in mitochondria, and its function is unknown. Mitochondria isolated from Fe-deficient cells contained $[Fe_4S_4]^{2+}$ clusters, low- and high-spin hemes, $S = {}^1/_2$ $[Fe_2S_2]^{+}$ clusters, NHHS Fe^{II} species, and $[Fe_2S_2]^{2+}$ clusters. The presence of $[Fe_2S_2]^{2+}$ clusters was unprecedented; their presence in previous samples was obscured by the spectroscopic signature of Fe^{III} nanoparticles, which are absent in Fe-deficient cells. Whether Fe-deficient cells were grown under fermenting or respirofermenting conditions had no effect on Fe content; such cells prioritized their use of Fe to essential forms devoid of nanoparticles and vacuolar Fe. The majority of Mn ions in wild-type yeast cells was electron paramagnetic resonance-active Mn^{II} and not located in mitochondria or vacuoles. Fermenting cells grown on Fe-sufficient and Fe-overloaded medium contained 400−450 μM Fe. In these cells, the concentration of nonmitochondrial NHHS Fe^{II} declined 3-fold, relative to that in Fe-deficient cells, whereas the concentration of vacuolar NHHS Fe^{III} increased to a limiting cellular concentration of ~300 μM. Isolated mitochondria contained more NHHS Fe^{II} ions and substantial amounts of Fe^{III} nanoparticles. The Fe contents of cells grown with excessive Fe in the medium were similar over a 250-fold change in nutrient Fe levels. The ability to limit Fe import prevents cells from becoming overloaded with Fe.

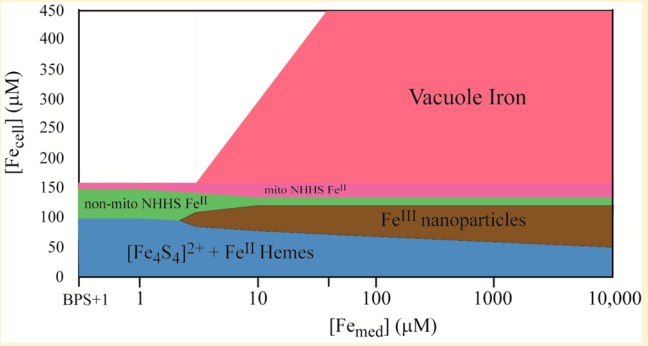

Iron plays critical roles in cells, including as redox agents within mitochondrial respiratory complexes and as an active-site metal in numerous metalloenzymes.[1−3] Iron can also be deleterious, in that certain types of Fe centers, e.g., labile mononuclear nonheme Fe^{II} complexes, engage in Fenton chemistry to generate reactive oxygen species (ROS). Thus, Fe trafficking in cells must be highly regulated to allow Fe to be used in cellular functions while also minimizing deleterious side processes. Understanding the molecular-level details of how cells do this is a current challenge in the field.

Cellular Fe trafficking involves numerous components interacting as a system. Membrane-bound proteins transport Fe across cellular and organellar membranes, while Fe-binding proteins and perhaps low-molecular mass Fe complexes traffic Fe within aqueous regions of the cell.[4] Iron-sensing proteins and DNA-binding transcription factors control gene expression levels of Fe-associated species,[5,6] while various chaperone proteins install Fe ions into myriad target/recipient apoproteins.

The details of Fe trafficking are best understood in the budding yeast *Saccharomyces cerevisiae*.[7] These cells import Fe through several pathways. A high-affinity pathway imports Fe through the Fet3p−Ftr1p complex on the plasma membrane. This pathway allows wild-type (WT) cells to grow under Fe-deficient conditions[8] in which the growth medium is pretreated with bathophenanthroline disulfonate (BPS), a strong chelator of Fe^{II} ions. The resulting $[Fe^{II}(BPS)_3]^{4-}$ complex, generated using endogenous Fe in the growth medium, is inaccessible to cells for growth.[9] WT cells growing in Fe-deficient medium express the iron regulon, a group of ~20 genes, including FET3 and FTR1.[10] Gene expression is controlled by transcription factor Aft1p.[5,6,11] Under Fe-deficient conditions, Aft1p moves from the cytosol to the nucleus where it increases the level of expression of iron regulon genes. Under Fe-sufficient and Fe-overload conditions, Aft1p moves to the cytosol, decreasing the expression of these genes. The rate of import of Fe into the cell by the high-affinity system is saturable, such that plots of rates versus the concentration of Fe in the medium ($[Fe_{med}]$) can be fit to a Michaelis−Menten-type expression with an apparent K_m of ~0.2 μM.[12−15]

Received: November 13, 2012
Revised: December 10, 2012
Published: December 19, 2012

Iron metabolism in cells grown under Fe-deficient conditions is also regulated post-transcriptionally. Cth1p and Cth2p bind to mRNA strands transcribed from various Fe-associated genes.[16] This destabilizes those transcripts and curtails protein synthesis. Cth2p binds and destabilizes the mRNA of Ccc1p, the only known Fe importer on the vacuolar membrane. Vacuoles store and detoxify Fe. These transcription factors also destabilize the mRNA of genes involved in Fe−S cluster and heme biosynthesis and respiration. Under Fe-deficient conditions, this regulatory mechanism minimizes the use of Fe by preventing vacuoles from depleting the cytosol of Fe and by curtailing synthesis of Fe-containing proteins.

Fe-sufficient growth conditions are defined here as having 5−40 μM ($[Fe_{med}]$). Cells lacking the high-affinity Fe import pathway can grow under such conditions[9,17] by using low-affinity pathways. Fe^{II} ions can be imported through Smf1p and Fet4p on the plasma membrane, with apparent K_m values of 2.2 and 33−41 μM, respectively.[13,18−20] Once imported, Fe is trafficked to vacuoles, mitochondria, and other organelles. CCC1 gene expression is controlled by transcription factor Yap5, which activates CCC1 at intermediate and high cytosolic Fe levels ($[Fe_{cyt}]$).[21] Once installed in the vacuolar membrane, the newly synthesized Ccc1p imports Fe into the vacuole.[22−24] Isolated vacuoles from fermenting cells grown at $[Fe_{med}]$ = 40 μM contain a magnetically isolated mononuclear HS Fe^{III} species.[25] In fermenting Fe-sufficient yeast cells, this species represents ∼75% of total cellular Fe.[26] Fe in vacuoles can also be found as Fe^{III} nanoparticles.[25,27] These organelles export Fe through Fet5p and Fth1p, homologues of Fet3p and Ftr1p,[28] and through Smf3p, a homologue of Smf1p.[29]

The same cytosolic Fe species that is imported into vacuoles[30] is presumed to be imported into mitochondria primarily through high-affinity transporters Mrs3p and Mrs4p.[31,32] High affinity in this case means that ΔMrs3/4 cells cannot grow on Fe-deficient medium,[31,33] apparently because $[Fe_{cyt}]$ in such cells is insufficient for Fe to be imported rapidly into mitochondria. Because mitochondria are the sole site of heme biosynthesis in the cell and the major site of Fe−S cluster biosynthesis, Fe-deficient ΔMrs3/4 cells probably cannot generate sufficient quantities of these prosthetic groups. These and other results imply that $[Fe_{cyt}]$ is proportional to $[Fe_{med}]$, at least under low-Fe conditions. These same strains can grow normally under Fe-sufficient conditions,[31] implying that low-affinity mitochondrial import pathways can operate when $[Fe_{cyt}]$ is higher than it is under Fe-deficient conditions.

Little is known about the Fe content and distribution in cells grown under Fe-overload growth conditions, defined here as being >40 μM $[Fe_{med}]$. Only at extremely high concentrations is toxicity observed. WT cells grow reasonably well in medium containing as much as 5−10 mM Fe^{II} and 20 mM Fe^{III}.[27,34−38]

We use an integrated biophysical approach centered on Mössbauer spectroscopy to evaluate the Fe content of organelles, cells, and tissues from a systems-level perspective.[25,39−41] In this paper, we analyze WT yeast cells grown on Fe-deficient and Fe-overloaded growth medium, as well as mitochondria isolated therefrom. Under Fe-deficient conditions, cells prioritize their use of Fe, using it for essential functions that involve Fe−S cluster and heme centers, and minimizing nanoparticles and vacuolar Fe. Cells grown at 40 to 10000 μM $[Fe_{med}]$ maintained nearly the same Fe concentration and speciation despite a 250-fold increase in the level of environmental Fe, indicating an amazing ability to regulate Fe import. A model that rationalizes these results is presented.

EXPERIMENTAL PROCEDURES

Cell Growth and Preparation of Samples. WT strain W303-1B and strain DY150 FET3-GFP::KanMX[42] were used. DY150 is isogenic to W303,[43] and it was used for studies involving Fet3-GFP. Cells were grown on minimal medium without added Fe,[26,44,45] called Fe-unsupplemented. The medium contained 2% (w/v) glucose or galactose to establish a fermenting or respirofermenting growth mode, respectively. Iron-deficient medium was prepared by adding 21 μM BPS (Sigma-Aldrich) to Fe-unsupplemented minimal medium, followed by supplementing with 1 μM ^{57}Fe citrate. This corresponded to a molar excess of BPS (the endogenous Fe concentration in minimal medium was ∼100 nM). We prepared ^{57}Fe citrate by dissolving ^{57}Fe metal powder (IsoFlex USA) in a 1:1 mixture of concentrated trace metal grade (TMG) HNO_3 and HCl (Fisher Scientific), and then diluting the mixture with doubly-distilled water. The resulting 80 mM Fe stock contained ∼0.2% (v/v) acid. The solution was diluted further with distilled water and treated with a 3-fold molar excess of sodium citrate (Fisher Scientific). The solution was adjusted to pH ∼5 with 1 M NaOH (EMD chemicals), resulting in a final ^{57}Fe citrate concentration of 40 mM.

Fifty milliliters of Fe-unsupplemented minimal medium was inoculated with a single colony from a YPAD (1% yeast extract, 2% peptone, 40 mg/L adenine sulfate, and 2% dextrose) plate. Cells were allowed to grow to an OD_{600} of 1.0−1.4 in a 30 °C rotary incubator at 150 rpm. The culture was used to inoculate fermenting minimal media supplemented with different concentrations of ^{57}Fe citrate. Once the OD_{600} reached 1.0−1.4, cells were collected by centrifugation at 4000*g* and rinsed 3× with 100 μM unbuffered EDTA. Subsequently, cells were rinsed 3× with water and packed into electron paramagnetic resonance (EPR) or Mössbauer cuvettes for analysis.

For cells from which mitochondria were isolated, 50 mL cultures were used to inoculate 1 L of growth medium. Once grown, these cultures were used to inoculate 24 L of medium in a custom glass bioreactor (ChemGlass) maintained at 30 °C. O_2 (99.99%) was bubbled through the bioreactor at 2 standard cubic feet per minute with a propeller rotation of 150 rpm. Cells were harvested at an OD_{600} of 1.0−1.4. Mitochondria were isolated as described previously[26] with EGTA (final concentration of 1 mM), present in all buffers. Samples were packed into EPR or Mössbauer cuvettes as described previously[24] and stored in LN_2 for subsequent analysis.

Spectroscopic Analysis. Mössbauer spectra were recorded using a model MS4 WRC spectrometer (SEE Co., Edina, MN) as described previously.[45] Parameters in the text are reported relative to α-Fe foil at room temperature (RT). Applied magnetic fields were parallel to the γ-radiation. Spectra were simulated using WMOSS. EPR spectra were recorded on an X-band spectrometer (EMX, Bruker Biospin Corp., Billerica, MA) with an Oxford Instruments ER910 cryostat. Spin quantifications used a 1.00 mM CuEDTA spin standard and SpinCount (http://www.chem.cmu.edu/groups/hendrich). UV−vis spectra were recorded at RT on a Hitachi 4400U spectrophotometer with a head-on photomultiplier tube. Spectra were analyzed as described for reduced heme *a*, *b*, and *c* content.[44]

Inductively Coupled Plasma Mass Spectrometry (ICP-MS) Analysis. Metal concentrations were determined by ICP-MS (Agilent model 7700x). Samples were packed into EPR cuvettes to determine the volume of the cell pellet (typically 200−300 μL). Following analysis by EPR, samples were diluted

dx.doi.org/10.1021/bi3015339 | *Biochemistry* 2013, 52, 105−114

by a known factor while being transferred to a 15 mL screw-top tube containing 100 μL of concentrated TMG HNO_3 (Fisher). Tubes were sealed with electrical tape to prevent evaporation and then incubated overnight at 90 °C. Digested samples were diluted with 7.8 mL doubly distilled H_2O and then analyzed by ICP-MS. Doubly distilled means that the H_2O was house-distilled, deionized using exchange columns (Thermo Scientific, model no. 09-034-3), and distilled again using a sub-boiling still (Savillex DST-1000).

Fet3-GFP Cells. Cells were grown to an OD_{600} of 1.0−1.2 on minimal medium supplemented with 21 μM BPS and various Fe concentrations under both fermenting and respiroferming conditions. Cells were harvested by centrifugation at 4000*g* and rinsed 3× with unbuffered EDTA (100 μM) and then 3× with water. A portion of the resulting material was saved for Western blot analysis; the remainder was packed into EPR or Mössbauer cuvettes. Protein concentrations were measured,[44] and 60 μg of protein of each sample was added per lane of an SDS−PAGE gel. Proteins were separated and transferred to a polyvinylidene difluoride membrane as described previously.[26] The membrane was then incubated with antibodies against GFP and actin (Thermo Scientific), with the actin serving as a loading control. OxyBlot assays were performed as suggested by the manufacturer (Millipore).

RESULTS

Iron-Deficient Cells. For this study, iron-deficient means that BPS was added to the growth medium to chelate endogenous unenriched Fe and that 1 μM $^{57}Fe^{III}$ citrate was subsequently added to enhance Mössbauer spectral intensity. Fe-deficient cells were grown with either glucose or galactose as the carbon source. Yeast cells exclusively ferment when grown on glucose, whereas they both respire and ferment (called respiroferming) when grown on galactose. In a previous study, we grew cells under respiroferming conditions using minimal medium supplemented with 40 μM ^{57}Fe.[44] The Fe content (i.e., the types of Fe centers and percentages of each type) of those cells was essentially indistinguishable from that of cells grown on glycerol, a respiration-only carbon source. Thus, at the resolution of our experiments, respirofermentation essentially mirrors respiration. Growing cells on galactose is more convenient than growing them on glycerol, so galactose-grown cells were used here. We will refer to BPS-treated fermenting and respiroferming cells as BPS-F and BPS-RF cells, respectively. We refer to fermenting cells grown with $[Fe_{med}]$ = 1, 10, 100, 1000 and 10000 μM as 1-F, 10-F, 100-F, 1000-F, and 10000-F, respectively.

Harvested BPS-F cells were rinsed with distilled and deionized water to remove $[Fe^{II}(BPS)_3]^{4-}$ and then packed into Mössbauer cups. The low-temperature (6 ± 1 K), low-field (0.05 T) Mössbauer spectrum of these pinkish cells (Figure S1A of the Supporting Information) exhibited a poor signal-to-noise (S/N) ratio because of the low ^{57}Fe concentration. An unresolved resonance in the center of the spectrum dominated. Authentic $[Fe^{II}(BPS)_3]^{4-}$ exhibited a similar feature (Figure S1B of the Supporting Information), suggesting that the BPS-F sample contained $[Fe^{II}(BPS)_3]^{4-}$ despite having been rinsed extensively. We subtracted the $[Fe^{II}(BPS)_3]^{4-}$ spectrum from that of the BPS-F cells, at 35% intensity, resulting in the spectrum shown in Figure 1B. Thus, only ∼65% of the total Fe in the packed sample (Table 1; 240 μM × 0.65 = 156 μM) was due to Fe contained in the BPS-F cells. Parenthetically, the

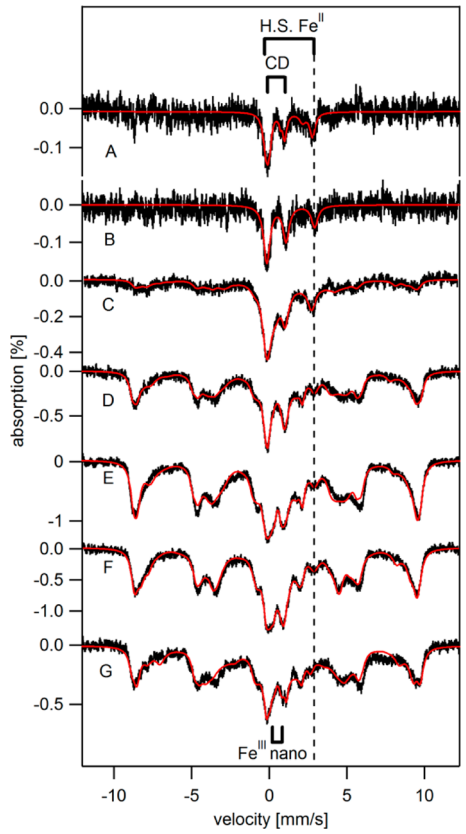

Figure 1. Mössbauer spectra (5−7 K, 0.05 T parallel field) of ^{57}Fe-enriched yeast cells at various $[Fe]_{med}$ values: (A) BPS-RF, (B) BPS-F, (C) 1-F, (D) 10-F, (E) 100-F, (F) 1000-F, and (G) 10000-F. Red lines are simulations assuming percentages given in Table 1. Brackets indicate the NHHS Fe^{II} doublet and the central doublet. Spectra A and B were obtained by subtracting contributions of the $[Fe^{II}(BPS)_3]^{4-}$ spectrum from the raw spectrum (shown in Figure S1A of the Supporting Information). Spectrum C has been published.[46] Red lines in spectra B−F are four-term simulations assuming the CD (δ = 0.45 mm/s, and ΔE_Q = 1.15 mm/s) and NHHS Fe^{II} doublets (δ = 1.3 mm/s, and ΔE_Q = 3.1 mm/s), a mononuclear HS Fe^{III} sextet, and a nanoparticle doublet (δ = 0.5 mm/s, and ΔE_Q = 0.6 mm/s). The HS Fe^{III} sextet was simulated using the following values: D = 0.5 cm^{-1}, E/D = 0.33, ΔE_Q = 0.10−0.14 mm/s, η = 2.8, $A_0/g_N \times \beta_N$ = −238 kG, δ = 0.54 mm/s, and Γ = 0.9 mm/s. The assumed temperatures for spectra C−G were 5, 6, 5, 7, and 6 K, respectively.

concentration of $[Fe^{II}(BPS)_3]^{4-}$ in the packed sample was substantially higher than the maximal possible concentration of $[Fe^{II}(BPS)_3]^{4-}$ in the medium (i.e., ∼0.1 μM), suggesting that $[Fe^{II}(BPS)_3]^{4-}$ collected on the cell's exterior. In principle, BPS could have penetrated the cell, but the charge on the complex probably discouraged this. Our packed pellets contain 70% cells and 30% buffer.[46] The concentrations listed in Table 1 have been corrected for this 0.7 packing efficiency.

The corrected BPS-F whole-cell Mössbauer spectrum was dominated by a quadruple doublet (δ = 0.45 mm/s, and ΔE_Q = 1.15 mm/s) indistinguishable from the central doublet (CD) identified previously.[47] This doublet arises from S = 0 $[Fe_4S_4]^{2+}$ clusters and LS Fe^{II} heme centers.[47] A second prominent feature was a quadrupole doublet with parameters typical of nonheme high-spin (NHHS) Fe^{II} (δ = 1.2 mm/s, and ΔE_Q = 3.1 mm/s). Percentages of these and all other spectral components are listed in Table 1. We estimate that the CD- and NHHS Fe^{II}-associated species in BPS-F cells are present at

dx.doi.org/10.1021/bi3015339 | *Biochemistry* 2013, 52, 105−114

Table 1. Characteristics of Isolated Mitochondria and Whole Cells[a]

whole cells	BPS-RF	BPS-F	1-F	10-F	100-F	1000-F	10000-F
$[Fe_{med}]$ (μM)	BPS + 1	BPS + 1	1	10	100	1000	10000
$[Fe]_{cell}$ (μM)	170 ± 50 (3)	240 ± 80 (3)	250 (1)	395 ± 40 (3)	470 ± 100 (3)	440 ± 80 (3)	450
$[Cu]_{cell}$ (μM)	62 ± 25 (3)	280 ± 20 (3)	–	26 ± 6 (3)	20 ± 6 (3)	35 ± 8 (3)	90
$[Mn]_{cell}$ (μM)	16 ± 7 (3)	17 ± 4 (3)	–	14 ± 4 (3)	17 ± 3 (3)	39 ± 10 (3)	30
$[Zn]_{cell}$ (μM)	160 ± 40 (3)	560 ± 70 (3)	–	600 ± 100 (3)	570 ± 70 (3)	1300 ± 130 (3)	300
NHHS Fe^{3+} (%)	~0	~0	40	76	80	75	84
CD (%)	43	36	22	18	10	5	3
NHHS Fe^{2+} (%)	39 (66 μM)	26 (62 μM)	26 (65 μM)	7 (26 μM)	5 (23 μM)	6 (26 μM)	5 (22 μM)
nanoparticles (%)	18	~ 0	12	~ 0	4	18	10
$[Fe^{2+}(BPS)_3]^{4-}$ (%)	12	35	N/A	N/A	N/A	N/A	N/A
g = 4.3 (μM)	~0	14	–	130	360	320	290
g = 2.0 region (μM)	26	14	–	16	15	28	27
mitochondria							
$[Fe]_{mito}$ (μM)	300	480 ± 160 (2)	–	544 ± 70 (2)	710 (1)	840 ± 200 (3)	500
$[Cu]_{mito}$ (μM)	270	80	–	48 ± 13 (2)	52 (1)	60 ± 20 (3)	65
$[Mn]_{mito}$ (μM)	12	13	–	12 ± 3 (2)	11 (1)	10 ± 2 (3)	22
$[Zn]_{mito}$ (μM)	250	570	–	236 ± 100 (2)	350 (1)	450 ± 200 (3)	150
NHHS Fe^{3+} (%)	ND	<15%	–	<15%	51, 0	–	–
CD (%)	63	59	–	11	12, 34	–	–
NHHS Fe^{2+} (%)	14	7	–	28	18, 36	–	–
HS Fe^{2+} heme (%)	7	9	–	~0	~0	–	–
nanoparticles (%)	ND	<10%	–	57	27	–	–
$S = 0$ $[Fe_2S_2]^{2+}$ (%)	ND	12	–	ND	ND	–	–
$S = {}^1/_2$ $[Fe_2S_2]^{+}$ (%)	ND	12	–	ND	ND	–	–
[g = 4.3] (μM)	ND	ND	–	20	20	28	–
[heme a] (μM)	30	30	–	24, 43	27	13	23
[heme b] (μM)	70	72	–	64, 58	78	21	40
[heme c] (μM)	120	120	–	110, 129	130	40	97

[a]Metal numbers, percentages used for Mössbauer spectral simulation, spin intensities of EPR signals, and concentrations of heme centers from UV–vis spectra. Percentages refer to Mössbauer spectra after removing the $[Fe^{II}(BPS)_3]^{4-}$ contribution. For fermenting mitochondria obtained from cells grown with 100 μM Fe in the medium, the two numbers listed for percentage refer to each of the two batches examined. EPR and ICP-MS data have been corrected for packing efficiency. Numbers in parentheses represent number of trials (n) if different from 1. Estimated uncertainties in Mössbauer percentages are ±4%, except for the sample obtained under Fe-deficient conditions in which the uncertainty is ±7%. Uncertainties for EPR spin quantifications are ±25%. Metal concentrations in cells have not been corrected for adventitious $[Fe^{II}(BPS)_3]^{4-}$ bound on the cell's exterior. ND, not determined; N/A, not applicable.

~90 and ~60 μM Fe, respectively. No other features, including those from Fe^{III} oxyhydroxide (phosphate) nanoparticles or mononuclear HS Fe^{III} species were evident, though minor contributions could have escaped detection because of the poor S/N ratio.

The corresponding Mössbauer spectrum of BPS-RF cells also exhibited a poor S/N ratio. In this case, a 12% contribution of the $[Fe^{II}(BPS)_3]^{4-}$ spectrum was subtracted, affording the corrected spectrum shown in Figure 1A. The spectrum was similar to that of BPS-F cells, including major contributions from CD and NHHS Fe^{II} features. The absolute concentrations of these features were also similar (73 and 66 μM, respectively). A minor feature arising from HS Fe^{II} hemes may be evident in the BPS-RF spectrum, but the low S/N ratio makes this assignment uncertain. In any event, the Mössbauer spectra of the two BPS-treated samples were very similar despite the fact that cells were grown in different metabolic modes.

EPR spectra of BPS-F and BPS-RF cells were also similar. Both exhibited low-intensity signals in the g = 2 region from Mn^{II} ions, as evidenced by the hyperfine splitting arising from the $I = {}^5/_2$ Mn nucleus (Figure 2A,B). Such signals were observed in all whole-cell spectra (Figure 2A–F) with similar intensities regardless of $[Fe_{med}]$. Also evident in the EPR spectra of BPS-F and BPS-RF cells were features at $g \approx 2.01$ and $g \approx 4.3$ and minor features in the g = 6 region. The g = 4.3 signal is due to mononuclear HS Fe^{III} ions with an E/D of ~$^1/_3$. The g = 6.4, 6.0, and 5.4 features originate from a partially oxidized state of cytochrome c oxidase.[47,48] No signals from Cu ions were observed, despite the relatively high concentration of Cu in all three BPS-F samples examined. Most Cu ions in these cells are probably in the diamagnetic Cu^I state, though there may be other reasons for the EPR silence.

Mitochondria from Fe-Deficient Cells. The pinkish color of the BPS-treated cells was absent in the corresponding isolated mitochondria, indicating that the $[Fe^{II}(BPS)_3]^{4-}$ complex that adhered to the cell exterior was removed during this process. The 6 K, 0.05 T Mössbauer spectrum of mitochondria isolated from BPS-F cells, called "BPS-F mitochondria" (Figure 3B), was dominated by the CD. Also present was a feature exhibiting magnetic hyperfine interactions that probably arose from $S = {}^1/_2$ $[Fe_2S_2]^{+}$ clusters, e.g., the cluster in the Rieske protein associated with cytochrome bc_1.[49] HS heme and nonheme Fe^{II} species were also present, as evidenced by the high-energy lines of the associated quadrupole doublets in the spectra.

BPS-F mitochondria were largely devoid of Fe^{III} oxyhydroxide nanoparticles, as the doublet caused by this species falls between the well-resolved lines of the CD. Indeed, the

dx.doi.org/10.1021/bi3015339 | Biochemistry 2013, 52, 105–114

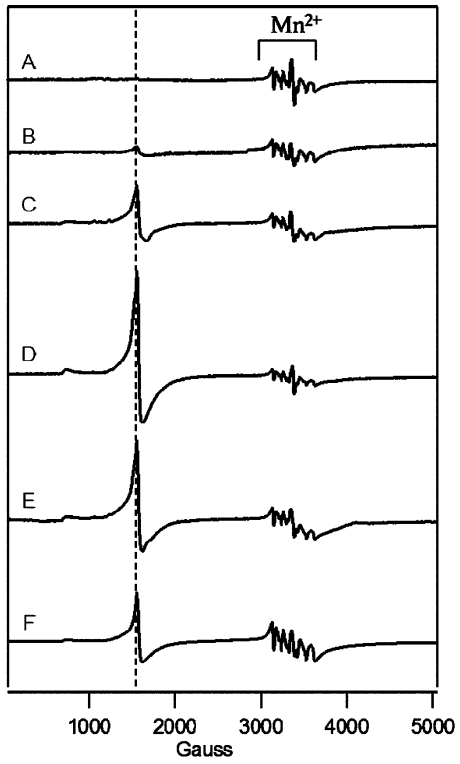

Figure 2. 10 K X-band EPR spectra of unenriched fermenting whole cells: (A) BPS-RF, (B) BPS-F, (C) 10-F, (D) 100-F, (E) 1000-F, and (F) 10000-F. Other EPR conditions: microwave frequency, 9.46 GHz; microwave power, 0.2 mW; modulation amplitude, 10 G; modulation frequency, 100 kHz; time constant, 335 s; sweep time, 165 s. The dashed line indicates the g = 4.3 feature.

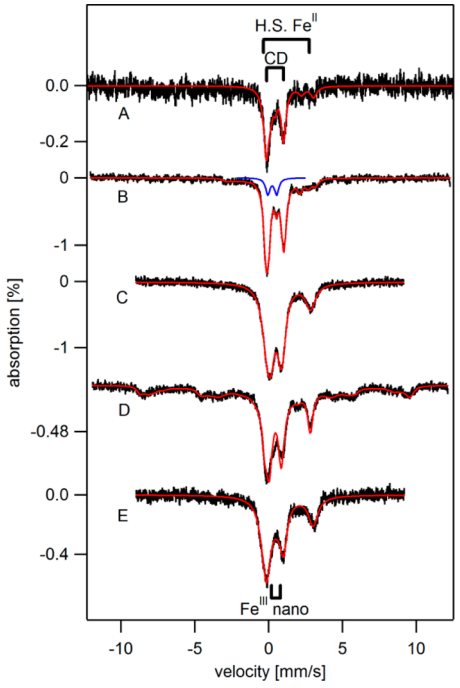

Figure 3. 6 K, 0.05 T Mössbauer spectra of isolated mitochondria from (A) BPS-RF cells, (B) BPS-F cells, (C) 10-F cells, (D) 100-F cells, and (E) 100-F cells with 1 mM dithionite added in 0.6 M sorbitol and 0.1 M Tris (pH 8.5). Red lines are simulations using percentages listed in Table 1. The blue line is a quadrupole doublet (δ = 0.3 mm/s, and ΔE_Q = 0.6 mm/s) typical of S = 0 $[Fe_2S_2]^{2+}$ clusters.

resolution between the CD lines was sufficient to discern a resonance near ~0.6 mm/s that was assigned to the high-energy line of a quadrupole doublet arising from S = 0 $[Fe_2S_2]^{2+}$ clusters. The blue line in Figure 3B is a simulation of that doublet. Such clusters in the oxidized diamagnetic +2 state have not been observed previously in any Mössbauer spectra of mitochondria, perhaps because previous spectra inevitably included contributions from nanoparticles[26,44] that absorb in the same region. The absence of intense NHHS Fe^{II} and nanoparticle doublets rendered the BPS-F spectrum more reminiscent of that obtained from 40-RF mitochondria,[44] which also lacked these doublets, than the spectrum of 40-F mitochondria that included them. However, even in 40-RF mitochondria, no feature arising from S = 0 $[Fe_2S_2]^{2+}$ clusters was discerned. Percentages used to fit the Figure 3B spectrum are given in Table 1.

The UV−vis spectrum of BPS-RF and BPS-F mitochondria (Figure 4A,B) exhibited features due to Fe^{II} heme centers. The

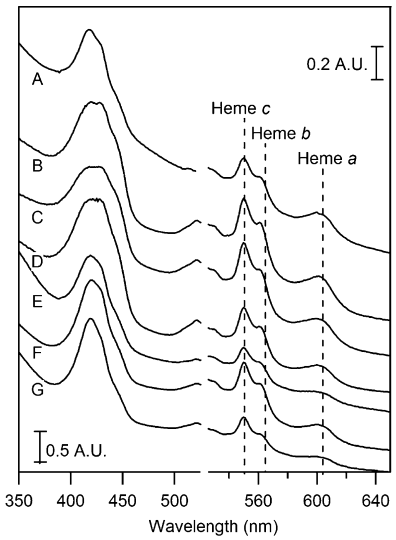

Figure 4. UV−vis spectra of isolated mitochondria: (A) BPS-RF, (B) BPS-F, (C) 10-F, (D) 100-F, (E) 1000-F, (F) 10-F from the second batch, and (G) 10000-F from the second batch.

concentrations of reduced hemes *a*, *b*, and *c* (Table 1) were similar to those reported for 40-R mitochondria.[44] The 10 K X-band EPR spectrum of BPS-RF and BPS-F mitochondria (Figure 5A,B) exhibited low-intensity g = 6.5, 5.4, and 4.3 signals. The first two signals probably arose from the a_3:Cu_b site of cytochrome *c* oxidase,[48] while the g = 4.3 signal arose from a rhombic HS Fe^{III} species in BPS-F mitochondria. The g = 2 region lacked the Mn^{II} signal that was evident in whole-cell spectra, indicating that the ions affording that signal are not located in mitochondria.

Fe-Sufficient Cells and Mitochondria. For comparison, we examined fermenting cells grown on medium supplemented with 1 μM (without BPS) and 10 μM ^{57}Fe. Mössbauer spectra of 1-F and 10-F cells (Figure 1C,D) exhibited features due to mononuclear HS Fe^{III}, the CD, NHHS Fe^{II}, and Fe^{III} oxyhydroxide nanoparticles (percentages given in Table 1). The main difference in these spectra was in the percentage of the HS Fe^{III} sextet. For 10-F cells, this percentage was more than double that in the 1-F spectrum. This feature undoubtedly arose from Fe within isolated vacuoles,[25] indicating that vacuolar Fe is essentially absent from BPS-F and BPS-RF

dx.doi.org/10.1021/bi3015339 | *Biochemistry* 2013, 52, 105−114

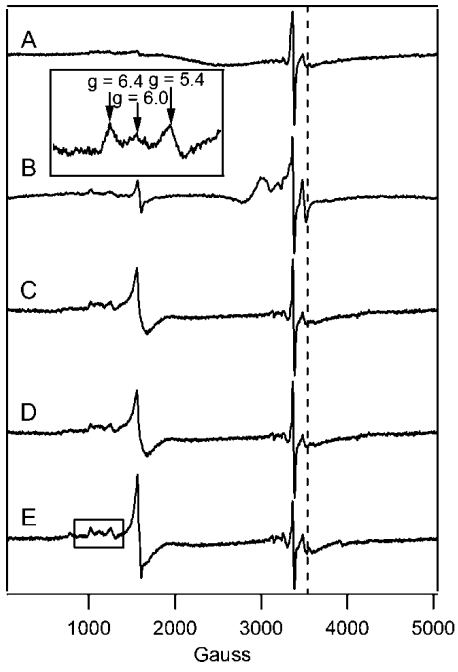

Figure 5. EPR of isolated mitochondria: (A) BPS-RF cells, (B) BPS-F cells, (C) 10-F cells, (D) 100-F cells, and (E) 1000-F cells. The samples used to generate A and B were those used to generate Figure 3A and Figure 3B, respectively. EPR conditions were as described in the legend of Figure 2. The dashed line indicates g = 1.94.

cells and that it starts to accumulate as cells grow in medium containing 1−10 μM Fe. ICP-MS analysis indicated that ∼100 μM Fe in 1-F cells and ∼300 μM Fe in 10-F cells were associated with vacuoles. This corresponds to 40 and 76% of cellular Fe, respectively.

EPR spectra of 10-F cells (Figure 2C) were generally similar to those of BPS-RF and BPS-F cells (spectra A and B, respectively, of Figure 2), except for a more pronounced $g \approx$ 4.3 signal. This is consistent with an increased concentration of the vacuolar mononuclear HS Fe^{III} species in the 10-F cells.

Interestingly, the absolute concentration of NHHS Fe^{II} ions in the cells (obtained by multiplying the cellular Fe concentration by the fractional Mössbauer intensity) decreased significantly (3-fold) as [Fe_{med}] increased from 1 to 10 μM. The average NHHS Fe^{II} concentration was 64 ± 2 μM in the BPS-F, BPS-RF, and 1-F samples, and 24 ± 2 μM in the 10-F, 100-F, 1000-F, and 10000-F cells (Table 1).

The low-temperature, low-field Mössbauer spectrum of 10-F mitochondria (Figure 3C) was nearly indistinguishable from that of 40-F mitochondria.[26] Relative to BPS-RF and BPS-F mitochondria, 10-F mitochondria exhibited considerably more Fe^{III} oxyhydroxide nanoparticles (Table 1). UV−vis (Figure 4C) and EPR (Figure 5C) spectra of 10-F mitochondria were also similar to those of 40-F mitochondria.[44] The UV−vis spectrum exhibited Fe^{II} heme concentrations similar to those seen in the BPS-F sample (Table 1). The concentration of Fe in the 10-F sample was reduced relative to that in the 40-F sample.

Fe-Overload Conditions. The Fe concentrations in 100-F, 1000-F, and 10000-F cells were similar to each other and to that of cells grown on 10 μM Fe (Table 1), despite the 1000-fold range of [Fe_{med}]. The Mössbauer spectra of these cells (Figure 1E−G) were also remarkably similar to each other and to spectra of 40-F cells; they exhibited similar contributions of the CD, the NHHS Fe^{II} doublet, and Fe^{III} nanoparticles. 100-F cells contained a slightly lower concentration of Fe^{III} nanoparticles than the other two samples. However, no general trend was apparent, in that the 1000-F sample exhibited a higher concentration of Fe^{III} nanoparticles than did 10000-F cells. The main point is that a 250-fold change in [Fe_{med}] (from 40 to 10000 μM) had little effect on the concentration or distribution of Fe within fermenting cells. One noticeable exception was a gradual but significant decline in the CD intensity as [Fe_{med}] increased (Table 1).

100-F, 1000-F, and 10000-F cells exhibited EPR spectra (spectra C−E, respectively, of Figure 2) similar to those of 10-F cells, except for more intense $g \approx$ 4.3 signals. Spin concentrations of the g = 4.3 signal (Table 1) represented ∼70% of the Fe concentration associated with the HS Fe^{III} sextet in the corresponding Mössbauer spectra. Although not a perfect match, this percentage indicates an acceptable congruence between the two types of measurements.

The 5 K, low-field Mössbauer spectra of isolated 10-F (Figure 3C), 40-F,[26] and 100-F mitochondria (Figure 3D) all included the CD, a HS Fe^{II} doublet, and a doublet due to Fe^{III} nanoparticles in approximately the same relative amounts. The 100-F sample also exhibited a sextet due to mononuclear HS Fe^{III} species representing ∼40% of the spectral intensity. 40-F mitochondria exhibited a similar feature but representing just 15% of the spectral intensity.[26]

The greater intensity of the sextet in the spectrum of 100-F mitochondria prompted us to consider whether the additional HS Fe^{III} ions were located in the mitochondria or whether they were an artifact of purification and bound on the exterior of the organelle. To address this, we isolated a second batch of 100-F mitochondria, including the reductant dithionite in the buffer. Dithionite does not appear to penetrate mitochondrial membranes.[26] The resulting spectrum (Figure 3E) showed no evidence of the sextet, suggesting that most or all of the Fe associated with this feature in the first sample was artifactual. The expense associated with preparing ^{57}Fe-enriched 100-F mitochondria from 24 L of cells prohibited us from exploring this issue further.

100-F and (unenriched) 1000-F mitochondria exhibited the same EPR signals with approximately the same relative intensities (Figure 5D,E). 10-F (Figure 5C) and 40-F[44] mitochondria exhibited very similar spectra. Importantly, the intensities of the g = 4.3 signal in the 100-F and 1000-F spectra were not higher than those in the 10-F or 40-F spectra. This is further evidence that the more intense HS Fe^{III} sextet observed in Mössbauer spectra of one batch of 100-F mitochondria was an artifact of that particular preparation. We conclude that the Fe contents of 10-F, 40-F, and 100-F mitochondria are approximately the same.

A sample of 100-F mitochondria exhibited a UV−vis spectrum (Figure 4D) similar to that of 10-F mitochondria (Figure 4C), while a 1000-F sample (Figure 4E) showed diminished intensities (heme concentrations given in Table 1). To address whether this decline reflected a cellular response to toxic levels of Fe in the growth medium, we isolated two batches of mitochondria, from cells grown with [Fe_{med}] values of 10 (control) and 10000 μM in the growth medium. Both batches of cells grew at nearly the same rate; i.e., the 10000 μM sample showed essentially no sign of toxicity. Oxyblot analysis of extracts of the two organelles (Figure S2 of the Supporting Information) indicated just 10% more ROS damage in the 10000-F sample relative to the 10-F sample. ICP-MS analysis

dx.doi.org/10.1021/bi3015339 | *Biochemistry* 2013, 52, 105−114

indicated insignificant differences in the concentration of Fe in the organelles (Table 1). However, corresponding UV−vis spectra indicated a decline in Fe^{II} heme intensities (Figure 4F,G and Table 1). The decline in heme intensity in panels E and G of Figure 4 appears to be real. We conclude that Fe concentrations in the growth medium as high as 10000 μM Fe^{III} citrate have insignificant effects on the growth rate of the cell, the level of ROS damage, and the Fe concentration of cells and their mitochondria and vacuoles. However, there does appear to be a decline in the level of $[Fe_4S_4]^{2+}$ clusters Fe^{II} hemes at very high $[Fe_{med}]$ values.

Fet3-GFP Expression Levels in Fermenting and Respiroferming Cells. The DY150 FET3-GFP::KanMX strain biosynthesizes the green fluorescent protein (GFP) fused to Fet3p.[42] We used this strain to perform a Western blot using an antibody against GFP as a reporter for Fet3p expression. The analysis was performed on cells grown under fermenting (and BPS-RF) conditions and supplemented with various concentrations of Fe in the growth medium. Fet3p was detected only in the BPS-F sample (Figure 6, right-most lane).

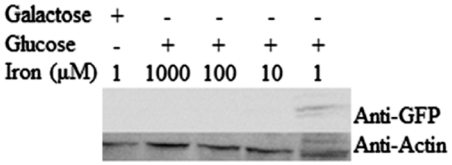

Figure 6. Western blot of Fet3-GFP cells grown under various conditions. Actin was added as a loading control. BPS was added to all samples.

Three bands were observed, with the middle band displaying the highest density. The upper band was ~7 times less intense but visible nevertheless. Because bands were not visible in any other lane, the concentration of Fet3-GFP in the BPS-F sample appears to have been at least 10 times greater than in the other samples, assuming no threshold effects. This suggests that the Aft1-controlled Fe regulon was effectively shut down when cells were grown in medium containing approximately >1 μM Fe. Fe-deficient respiroferming cells do not appear to utilize the Fe regulon, as no Fet3p expression was observed.

DISCUSSION

Fe-Deficient State. Fermenting WT yeast cells grown under Fe-deficient conditions prioritize their use of Fe for essential functions. Such cells were devoid of vacuolar HS Fe^{III}, a storage form of Fe that is not essential, and were largely devoid of Fe^{III} oxyhydroxide (phosphate or polyphosphate) nanoparticles, which do not seem to function in cellular Fe metabolism. Fe-deficient cells had a total Fe concentration of ~150 μM, distributed into two major groups. Approximately 80 μM was present as $S = 0$ $[Fe_4S_4]^{2+}$ clusters and LS Fe^{II} hemes (the two types of Fe cannot be distinguished by Mössbauer), most of which are undoubtedly associated with mitochondria and respiration. Approximately 60 μM cellular Fe corresponded to NHHS Fe^{II} species. Approximately the same distribution of Fe was observed in both fermenting and respiroferming Fe-deficient cells.

Mitochondria from Fe-deficient fermenting and respiroferming cells also prioritize their use of Fe; they contained similar levels of respiratory complexes relative to Fe-sufficient mitochondria but lower concentrations of nanoparticles and NHHS Fe^{II}/Fe^{III} species. This distribution was more typical of

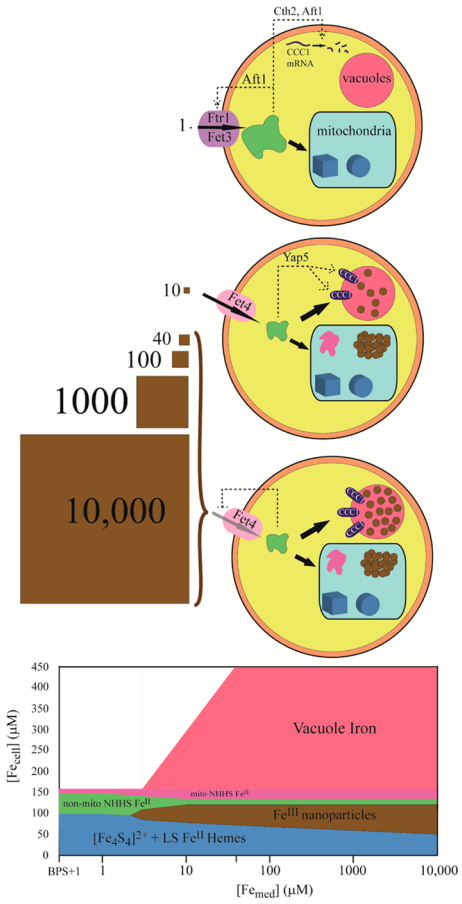

Figure 7. Model of the distribution and regulation of Fe in fermenting yeast cells: (top) Fe-deficient, (middle) Fe-sufficient, and (bottom) Fe-loaded. The concentration of Fe^{III} citrate in the growth medium (in micromolar) is indicated by the brown squares. Two import pathways are shown, including the high-affinity pathway (Aft1 regulating the iron regulon, including Fet3p) and the low-affinity pathway (Fet4p-based). Also shown are mitochondria (blue rectangular shape) and vacuoles (red sphere). Under Fe-deficient conditions, Fe is imported via the high-affinity pathway; a portion is imported into mitochondria where Fe−S clusters (brown cube) and heme centers (disks) are predominantly made. Most of the rest of the imported Fe is present as a nonmitochondrial NHHS Fe^{II} pool (shown here in the cytosol, but this is not known). Aft1p is sensing a small portion of this pool. The vacuoles are empty because Cth2 working with Aft1p is activated by the absence of cytosolic Fe to degrade CCC1 mRNA. Under Fe-sufficient conditions, the high-affinity pathway is shut down and the majority of Fe is imported via the low-affinity pathway. The concentration of nonmitochondrial NHHS Fe^{II} is reduced 3-fold, perhaps because a portion is imported into mitochondria and converted to nanoparticles (clumps of brown circles) and NHHS Fe^{II} and Fe^{III}. The vacuoles are partially filled with mononuclear HS Fe^{III} species, because of the absence of the Cth2 effect and the presence of Yap5p-dependent expression of CCC1. Under Fe-overload conditions, the Fe content is similar to that under Fe-sufficient conditions except that the vacuoles are filled completely. The low-affinity import pathway is saturable such that a 250-fold change in the Fe concentration of the medium does not significantly impact the cellular Fe content. The bottom panel summarizes these changes. Percentages of various species are approximate, and minor unassigned species are not included.

Fe-sufficient mitochondria from respiring cells.[44] We previously proposed that the NHHS Fe^{II} and Fe^{III} species in mitochondria are in equilibrium with each other and with the nanoparticles

dx.doi.org/10.1021/bi3015339 | Biochemistry 2013, 52, 105−114

contained therein, and that the NHHS Fe^{II} species constitutes a pool of Fe used for heme and Fe−S cluster biosynthesis.[26] The size of this pool shrinks in respiring mitochondria, which is consistent with the higher rates of Fe−S cluster and heme biosynthesis. The lower concentrations of this pool observed in Fe-deficient mitochondria might arise instead from a diminished rate of import of Fe from the cytosol into mitochondria caused by low cytosolic Fe concentrations.

A Nonmitochondrial NHHS Fe^{II} Pool. The concentration of NHHS Fe^{II} in isolated Fe-deficient mitochondria was ∼40 μM. What proportion of the NHHS Fe^{II} pool observed in whole cells is due to the NHHS Fe^{II} species in mitochondria? Mitochondria in fermenting cells occupy between 3 and 10% of the cell volume.[50] This means that the concentration of mitochondrially associated NHHS Fe^{II} species in Fe-deficient cells is 1.2−4 μM (i.e., 40 μM × 0.03−0.1). Because the observed concentration of NHHS Fe^{II} in Fe-deficient whole cells was ∼60 μM, we conclude that >90% of the NHHS Fe^{II} in whole cells is not located in mitochondria. This nonmitochondrial pool also does not appear to be located in vacuoles.[25] As a working hypothesis, we propose that the pool of NHHS Fe^{II} in Fe-deficient cells is located in the cytosol.

Decrease in the Level of Nonmitochondrial NHHS Fe^{II} as [Fe_{med}] Increases. Under Fe-sufficient and Fe-overload conditions, mitochondria contained ∼150 μM NHHS Fe^{II}, a 3-fold increase relative to that under Fe-deficient conditions. Under these high-Fe conditions, our calculations suggest that as much as 60% of the NHHS Fe^{II} species present in whole cells is now located in mitochondria. Thus, the decline of nonmitochondrial NHHS Fe^{II} as cells undergo the transition from being Fe-deficient to Fe-sufficient (from 60 to 25 μM) is more dramatic than implied by the 60:25 ratio. These results suggest that during the transition in [Fe_{med}] from 1 to 10 μM, most of the nonmitochondrial (probably cytosolic) NHHS Fe^{II} species of whole Fe-deficient cells move into the mitochondria where they contribute to the NHHS Fe^{II} pool (and ultimately nanoparticles) in this organelle.

Occurring in approximately the same transition period was a decline in the level of expression of the Fe regulon as reported by Fet3p, confirming previous studies that Aft1-dependent expression of the Fe regulon is effectively abolished when [Fe_{med}] >1 μM.[10,51] The low-affinity pathways play the major role in regulating cellular Fe beyond this transition. The transition of nonmitochondrial NHHS Fe^{II} into the mitochondria (or vacuoles) might be related to the switch from high- to low-affinity Fe regulatory mechanisms or to the activation of CCC1.

Accumulation of Vacuolar Fe. The lack of vacuolar Fe in Fe-deficient cells is probably due to the lack of Ccc1p on the vacuole membrane caused by destabilization of CCC1 mRNA by Cth1p and Cth2p under Fe-deficient conditions (the process also requires Aft1p and Aft2p).[52] Cth1p and Cth2p also destabilize the mRNA of genes involved in Fe−S cluster and heme biosynthesis and the mRNA of numerous Fe−S cluster-containing and heme-containing proteins. Our results support previous studies regarding the effects of Cth1p and Cth2p on CCC1p but do not indicate lower concentrations of Fe−S cluster or heme centers in Fe-deficient cells or mitochondria. This is probably because we supplemented the BPS-treated medium with 1 μM ^{57}Fe (to allow Mössbauer analysis), which rendered our cells less rigorously Fe-deficient than the BPS-treated cells of Thiele and co-workers.[21] We suspect that their Fe-starved cells shut down Fe−S cluster and heme assembly in a final attempt to survive.

The level of CCC1 gene expression increases dramatically between [Fe_{med}] values of 5 and 50 μM,[21] consistent with the increased level of vacuole Fe that we observed as [Fe_{med}] increased. In this case, the increased level of CCC1 expression is probably due to Yap5p. As the concentration of Ccc1p on the vacuolar membrane increases, vacuoles import Fe such that the vacuoles in cells grown on 1, 10, and 40 μM Fe are ∼0, ∼40, and ∼100% filled, respectively.

The concentration of Fe that can be associated with vacuoles is maximal between 300 and 350 μM. We have previously estimated that the Fe concentration in vacuoles in cells grown on 40 μM Fe is ∼1.2 mM, based on the assumption that these organelles occupy ∼25% of the cell volume.[26,46] Our results indicate that cells limit the storage of HS Fe^{III} in vacuoles to this cellular Fe concentration, regardless of the concentration of Fe in the growth medium. Whether they do this by limiting the percentage volume of vacuoles in the cell and/or the concentration of mononuclear HS Fe^{III} contained therein is uncertain.

The total Fe concentration in fermenting cells is also limited, with a minimum of ∼160 μM in Fe-deficient cells. This concentration gradually increases as vacuoles fill and other changes occur, becoming maximal at ∼450 μM in cells grown in Fe-overloaded medium. The increase in cellular Fe concentration is largely (but not entirely) due to the vacuoles filling with Fe, suggesting that the Fe concentrations of all nonvacuolar Fe components of the cell are roughly invariant (at ∼160 μM) during this process. The majority of this invariant portion of cellular Fe is mitochondrial.

Modest Changes in the Distribution of Fe in the Cells Grown on Fe-Overloaded Medium. The concentration of Fe in cells and the distribution of that Fe into different groups are roughly invariant over a 250-fold range of [Fe_{med}] (from 40 to 10000 μM). In this region, Fe is being imported via low-affinity pathways. The invariant Fe concentration suggests that the low-affinity pathway must be saturated throughout this 250-fold interval. The Fe import velocity might be saturable, in which case a Michaelis−Menten-like expression with a $K_{m\text{-}app}$ of ∼15 μM Fe could simulate this effect. This is within a factor of 2 of previous estimates of the apparent K_m for the low-affinity transporter.[13,19,20] Our results also reveal why WT yeast cells grow well under high-Fe (5−10 mM) conditions, namely that they prevent excess environmental Fe from being imported (rather than, for example, having special mechanisms to detoxify excess imported Fe).

Two modest but noticeable changes in the Fe distribution of such cells were the declines in the concentration of Fe associated with the Mössbauer central doublet and heme centers as [Fe_{med}] increased. Under Fe-deficient conditions, the cellular CD concentration was ∼80 μM, whereas with [Fe_{med}] values of 1, 10, 100, 1000, and 10000 μM, it was 55, 71, 47, 22, and 14 μM, respectively. UV−vis spectra also showed some decline in heme features at high medium Fe concentrations. These declines might reflect a decline in the fractional cellular volume occupied by mitochondria or a decline in the concentration of Fe-rich respiratory complexes. More extreme declines of these centers under even higher medium Fe concentrations might be responsible for the Fe-associated toxicity that is eventually observed.

Cellular Manganese. Comparing the ICP-MS-detected Mn concentrations to the spin concentrations of the Mn-

associated EPR signal [g = 2.0 region (Table 1)] indicates that the majority of Mn ions in the cells are mononuclear Mn^{II} species that exhibit the EPR signal. This differs from the study of Chang and Kosman,[53] who reported that the majority of cellular Mn is EPR-silent. McNaughton et al. used ENDOR spectroscopy to investigate the species affording this signal[54] and determined that >70% of the contributing species are Mn^{II} ions coordinated with phosphate and/or polyphosphate anions. The absence of these signals in isolated mitochondria and vacuoles[25] suggests that these Mn^{II}(phosphate/polyphosphate) species are not located in either of these organelles. The concentration of Mn^{II}(phosphate/polyphosphate) species in our fermenting yeast cells appears to be 10−30 μM, regardless of [Fe_{med}].

Summary Model. The major results of this study can be summarized by the model shown in Figure 7. The high-affinity Fe import pathway operates at [Fe_{med}] values of approximately ≤1 μM (BPS-treated with 1 μM ^{57}Fe). Under these conditions, the cell is Fe-deficient and must prioritize its use of Fe. Most of this precious commodity goes to the mitochondria where it is assembled into Fe−S clusters and heme centers, prosthetic groups that are critical for cellular metabolism. Little Fe is stored in vacuoles, and little is present as Fe^{III} nanoparticles. A significant portion of cellular Fe in Fe-deficient cells is in the form of NHHS Fe^{II} and is probably located in the cytosol. When [Fe_{med}] ∼ 10 μM, the high-affinity pathway is shut down and Fe is regulated by low-affinity pathways. The mitochondria remain the sites where much imported Fe is sent for Fe−S cluster and heme synthesis. Additional Fe is imported (perhaps from the cytosolic pool of NHHS Fe^{II}), increasing the size of the pool of mitochondrial NHHS Fe^{II} and Fe^{III} oxyhydroxide nanoparticles. The level of cytosolic NHHS Fe^{II} species declines as some becomes stored in vacuoles as nonheme HS Fe^{III} species. When [Fe_{med}] = 40−10000 μM, the vacuoles are filled with Fe, and little else changes in terms of Fe content and distribution. The low-affinity import pathways are saturated in accordance with apparent K_m values of 15−30 μM, limiting Fe import at this and higher [Fe_{med}] values. This prevents high concentrations of environmental Fe from entering the cell and causing toxicity. These regulatory properties allow fermenting yeast cells to grow on medium with Fe concentrations that vary over 4 orders of magnitude, an impressive feat by any standard!

■ ASSOCIATED CONTENT

Supporting Information

Mössbauer spectra showing the contribution of BPS in Fe-deficient cells (Figure S1) and an Oxyblot analysis of mitochondria isolated from WT cells grown under different Fe conditions (Figure S2). This material is available free of charge via the Internet at http://pubs.acs.org.

■ AUTHOR INFORMATION

Corresponding Author

*Phone: (979) 845-0956. Fax: (979) 845-4719. E-mail: Lindahl@chem.tamu.edu.

Funding

This study was sponsored by the National Institutes of Health (GM084266) and the Robert A. Welch Foundation (A1170).

Notes

The authors declare no competing financial interest.

■ ACKNOWLEDGMENTS

We thank Jerry Kaplan (University of Utah, Salt Lake City, UT) for kindly providing the DY150 FET3-GFP::KanMX strain.

■ REFERENCES

(1) Ye, H., and Rouault, T. A. (2010) Human Iron-Sulfur Cluster Assembly, Cellular Iron Homeostasis, and Disease. *Biochemistry 49*, 4945−4956.

(2) Lill, R. (2009) Function and biogenesis of iron-sulphur proteins. *Nature 460*, 831−838.

(3) Kaplan, C. D., and Kaplan, J. (2009) Iron Acquisition and Transcriptional Regulation. *Chem. Rev. 109*, 4536−4552.

(4) Jacobs, A. (1977) Low molecular weight intracellular iron transport compounds. *Blood 50*, 433−439.

(5) Casas, C., Aldea, M., Espinet, C., Gallego, C., Gil, R., and Herrero, E. (1997) The AFT1 transcriptional factor is differentially required for expression of high-affinity iron uptake genes in *Saccharomyces cerevisiae*. *Yeast 13*, 621−637.

(6) Rutherford, J. C., Jaron, S., and Winge, D. R. (2003) Aft1p and Aft2p mediate iron-responsive gene expression in yeast through related promoter elements. *J. Biol. Chem. 278*, 27636−27643.

(7) Philpott, C. C. (2006) Iron uptake in fungi: A system for every source. *Biochim. Biophys. Acta 1763*, 636−645.

(8) Davis-Kaplan, S. R., Ward, D. M., Shiflett, S. L., and Kaplan, J. (2004) Genome-wide Analysis of Iron-dependent Growth Reveals a Novel Yeast Gene Required for Vacuolar Acidification. *J. Biol. Chem. 279*, 4322−4329.

(9) Eide, D., Daviskaplan, S., Jordan, I., Sipe, D., and Kaplan, J. (1992) Regulation of Iron Uptake in *Saccharomyces cerevisiae*: The Ferrireductase and Fe(II) Transporter Are Regulated Independently. *J. Biol. Chem. 267*, 20774−20781.

(10) Yamaguchi-Iwai, Y., Stearman, R., Dancis, A., and Klausner, R. D. (1996) Iron-regulated DNA binding by the AFT1 protein controls the iron regulon in yeast. *EMBO J. 15*, 3377−3384.

(11) Courel, M., Lallet, S., Camadro, J. M., and Blaiseau, P. L. (2005) Direct activation of genes involved in intracellular iron use by the yeast iron-responsive transcription factor Aft2 without its paralog Aft1. *Mol. Cell. Biol. 25*, 6760−6771.

(12) Dancis, A., Roman, D. G., Anderson, G. J., Hinnebusch, A. G., and Klausner, R. D. (1992) Ferric Reductase of *Saccharomyces cerevisiae*: Molecular Characterization, Role in Iron Uptake, and Transcriptional Control by Iron. *Proc. Natl. Acad. Sci. U.S.A. 89*, 3869−3873.

(13) Dix, D., Bridgham, J., Broderius, M., and Eide, D. (1997) Characterization of the FET4 protein of yeast: Evidence for a direct role in the transport of iron. *J. Biol. Chem. 272*, 11770−11777.

(14) Askwith, C., Eide, D., Vanho, A., Bernard, P. S., Li, L. T., Daviskaplan, S., Sipe, D. M., and Kaplan, J. (1994) The Fet3 Gene of *Saccharomyces cerevisiae* Encodes a Multicopper Oxidase Required for Ferrous Iron Uptake. *Cell 76*, 403−410.

(15) Desilva, D. M., Askwith, C. C., Eide, D., and Kaplan, J. (1995) The Fet3 Gene-Product Required for High-Affinity Iron Transport in Yeast Is a Cell-Surface Ferroxidase. *J. Biol. Chem. 270*, 1098−1101.

(16) Puig, S., Vergara, S. V., and Thiele, D. J. (2008) Cooperation of two mRNA-binding proteins drives metabolic adaptation to iron deficiency. *Cell Metab. 7*, 555−564.

(17) Askwith, C., Eide, D., Van Ho, A., Bernard, P. S., Li, L., Davis-Kaplan, S., Sipe, D. M., and Kaplan, J. (1994) The FET3 gene of *S. cerevisiae* encodes a multicopper oxidase required for ferrous iron uptake. *Cell 76*, 403−410.

(18) Chen, X.-Z., Peng, J.-B., Cohen, A., Nelson, H., Nelson, N., and Hediger, M. A. (1999) Yeast SMF1 Mediates H^+-coupled Iron Uptake with Concomitant Uncoupled Cation Currents. *J. Biol. Chem. 274*, 35089−35094.

(19) Hassett, R., Dix, D. R., Eide, D. J., and Kosman, D. J. (2000) The Fe(II) permease Fet4p functions as a low affinity copper

transporter and supports normal copper trafficking in *Saccharomyces cerevisiae*. *Biochem. J. 351* (Part 2), 477−484.
(20) Dix, D. R., Bridgham, J. T., Broderius, M. A., Byersdorfer, C. A., and Eide, D. J. (1994) The FET4 gene encodes the low affinity Fe(II) transport protein of *Saccharomyces cerevisiae*. *J. Biol. Chem. 269*, 26092−26099.
(21) Li, L., Bagley, D., Ward, D. A., and Kaplan, J. (2008) Yap5 is an iron-responsive transcriptional activator that regulates vacuolar iron storage in yeast. *Mol. Cell. Biol. 28*, 1326−1337.
(22) Li, L. T., Chen, O. S., Ward, D. M., and Kaplan, J. (2001) A yeast vacuolar membrane transporter CCC1 facilitates iron storage. *Mol. Biol. Cell 12*, 206a.
(23) Kaplan, C. D., and Kaplan, J. (2009) Iron acquisition and transcriptional regulation. *Chem. Rev. 109*, 4536−4552.
(24) Lindahl, P. A., Morales, J. G., Miao, R., and Holmes-Hampton, G. (2009) Isolation of *Saccharomyces cerevisiae* Mitochondria for Mössbauer, EPR, and Electronic Absorption Spectroscopic Analyses. *Methods Enzymol. 456*, 267−285.
(25) Cockrell, A. L., Holmes-Hampton, G. P., McCormick, S. P., Chakrabarti, M., and Lindahl, P. A. (2011) Mössbauer and EPR Study of Iron in Vacuoles from Fermenting *Saccharomyces cerevisiae*. *Biochemistry 50*, 10275−10283.
(26) Holmes-Hampton, G. P., Miao, R., Morales, J. G., Guo, Y. S., Münck, E., and Lindahl, P. A. (2010) A Nonheme High-Spin Ferrous Pool in Mitochondria Isolated from Fermenting *Saccharomyces cerevisiae*. *Biochemistry 49*, 4227−4234.
(27) Nishida, K., and Silver, P. A. (2012) Induction of Biogenic Magnetization and Redox Control by a Component of the Target of Rapamycin Complex 1 Signaling Pathway. *PLoS Biol. 10*, e1001269.
(28) Urbanowski, J. L., and Piper, R. C. (1999) The iron transporter fth1p forms a complex with the Fet5 iron oxidase and resides on the vacuolar membrane. *J. Biol. Chem. 274*, 38061−38070.
(29) Portnoy, M. E., Liu, X. F., and Culotta, V. C. (2000) *Saccharomyces cerevisiae* expresses three functionally distinct homologues of the Nramp family of metal transporters. *Mol. Cell. Biol. 20*, 7893−7902.
(30) Li, L. T., and Kaplan, J. (2004) A mitochondrial-vacuolar signaling pathway in yeast that affects iron and copper metabolism. *J. Biol. Chem. 279*, 33653−33661.
(31) Mühlenhoff, U., Stadler, J. A., Richhardt, N., Seubert, A., Eickhorst, T., Schweyen, R. J., Lill, R., and Wiesenberger, G. (2003) A specific role of the yeast mitochondrial carriers Mrs3/4p in mitochondrial iron acquisition under iron-limiting conditions. *J. Biol. Chem. 278*, 40612−40620.
(32) Froschauer, E. M., Schweyen, R. J., and Wiesenberger, G. (2009) The yeast mitochondrial carrier proteins Mrs3p/Mrs4p mediate iron transport across the inner mitochondrial membrane. *Biochim. Biophys. Acta 1788*, 1044−1050.
(33) Foury, F., and Roganti, T. (2002) Deletion of the mitochondrial carrier genes MRS3 and MRS4 suppresses mitochondrial iron accumulation in a yeast frataxin-deficient strain. *J. Biol. Chem. 277*, 24475−24483.
(34) Jo, W. J., Loguinov, A., Chang, M., Wintz, H., Nislow, C., Arkin, A. P., Giaever, G., and Vulpe, C. D. (2008) Identification of genes involved in the toxic response of *Saccharomyces cerevisiae* against iron and copper overload by parallel analysis of deletion mutants (vol 101, pg 140, 2008). *Toxicol. Sci. 102*, 205−205.
(35) Kucej, M., and Foury, F. (2003) Iron toxicity protection by truncated Ras2 GTPase in yeast strain lacking frataxin. *Biochem. Biophys. Res. Commun. 310*, 986−991.
(36) Lee, A., Henras, A. K., and Chanfreau, G. (2005) Multiple RNA surveillance pathways limit aberrant expression of iron uptake mRNAs and prevent iron toxicity in *S. cerevisiae*. *Mol. Cell 19*, 39−51.
(37) Bleackley, M. R., Young, B. P., Loewen, C. J. R., and MacGillivray, R. T. A. (2011) High density array screening to identify the genetic requirements for transition metal tolerance in *Saccharomyces cerevisiae*. *Metallomics 3*, 195−205.
(38) Peiter, E., Fischer, M., Sidaway, K., Roberts, S. K., and Sanders, D. (2005) The *Saccharomyces cerevisiae* Ca^{2+} channel Cch1pMid1p is essential for tolerance to cold stress and iron toxicity. *FEBS Lett. 579*, 5697−5703.
(39) Lindahl, P. A., and Holmes-Hampton, G. P. (2011) Biophysical probes of iron metabolism in cells and organelles. *Curr. Opin. Chem. Biol. 15*, 342−346.
(40) Jhurry, N. D., Chakrabarti, M., McCormick, S. P., Holmes-Hampton, G. P., and Lindahl, P. A. (2012) Biophysical investigation of the ironome of human Jurkat cells and mitochondria. *Biochemistry 51*, 5276−5284.
(41) Holmes-Hampton, G. P., Chakrabarti, M., Cockrell, A. L., McCormick, S. P., Abbott, L. C., Lindahl, L. S., and Lindahl, P. A. (2012) Changing iron content of the mouse brain during development. *Metallomics 4*, 761−770.
(42) Felice, M. R., De Domenico, I., Li, L. T., Ward, D. M., Bartok, B., Musci, G., and Kaplan, J. (2005) Post-transcriptional regulation of the yeast high affinity iron transport system. *J. Biol. Chem. 280*, 22181−22190.
(43) Thomas, B. J., and Rothstein, R. (1989) Elevated Recombination Rates in Transcriptionally Active DNA. *Cell 56*, 619−630.
(44) Garber Morales, J., Holmes-Hampton, G. P., Miao, R., Guo, Y., Münck, E., and Lindahl, P. A. (2010) Biophysical characterization of iron in mitochondria isolated from respiring and fermenting yeast. *Biochemistry 49*, 5436−5444.
(45) Miao, R., Martinho, M., Morales, J. G., Kim, H., Ellis, E. A., Lill, R., Hendrich, M. P., Münck, E., and Lindahl, P. A. (2008) EPR and Mössbauer spectroscopy of intact mitochondria isolated from Yah1p-depleted *Saccharomyces cerevisiae*. *Biochemistry 47*, 9888−9899.
(46) Miao, R., Holmes-Hampton, G. P., and Lindahl, P. A. (2011) Biophysical Investigation of the Iron in Aft1-1(up) and Gal-YAH1 *Saccharomyces cerevisiae*. *Biochemistry 50*, 2660−2671.
(47) Hudder, B. N., Morales, J. G., Stubna, A., Münck, E., Hendrich, M. P., and Lindahl, P. A. (2007) Electron paramagnetic resonance and Mössbauer spectroscopy of intact mitochondria from respiring *Saccharomyces cerevisiae*. *J. Biol. Inorg. Chem. 12*, 1029−1053.
(48) Aasa, R., Albracht, S. P. J., Falk, K.-E., Lanne, B., and Vänngård, T. (1976) EPR signals from cytochrome c oxidase. *Biochim. Biophys. Acta 422*, 260−272.
(49) Fee, J. A., Findling, K. L., Yoshida, T., Hille, R., Tarr, G. E., Hearshen, D. O., Dunham, W. R., Day, E. P., Kent, T. A., and Münck, E. (1984) Purification and characterization of the Rieske iron-sulfur protein from *Thermus thermophilus*. Evidence for a [2Fe-2S] cluster having non-cysteine ligands. *J. Biol. Chem. 259*, 124−133.
(50) Stevens, B. J. (1977) Variation in Number and Volume of Mitochondria in Yeast According to Growth-Conditions: Study Based on Serial Sectioning and Computer Graphics Reconstitution. *Biol. Cell. 28*, 37−56.
(51) Yamaguchi-Iwai, Y., Dancis, A., and Klausner, R. D. (1995) AFT1: A mediator of iron regulated transcriptional control in *Saccharomyces cerevisiae*. *EMBO J. 14*, 1231−1239.
(52) Puig, S., Askeland, E., and Thiele, D. J. (2005) Coordinated remodeling of cellular metabolism during iron deficiency through targeted mRNA degradation. *Cell 120*, 99−110.
(53) Chang, E. C., and Kosman, D. J. (1989) Intracellular Mn(II)-associated superoxide scavenging activity protects Cu,Zn superoxide dismutase-deficient *Saccharomyces cerevisiae* against dioxygen stress. *J. Biol. Chem. 264*, 12172−12178.
(54) McNaughton, R. L., Reddi, A. R., Clement, M. H. S., Sharma, A., Barnese, K., Rosenfeld, L., Gralla, E. B., Valentine, J. S., Culotta, V. C., and Hoffman, B. M. (2010) Probing in vivo Mn^{2+} speciation and oxidative stress resistance in yeast cells with electron-nuclear double resonance spectroscopy. *Proc. Natl. Acad. Sci. U.S.A. 107*, 15335−15339.